Chem Biol Drug Des 2006; **68:** 239–249

doi: 10.1111/j.1747-0285.2006.00444.x

Research Article

Interactions between Conserved Residues in Transmembrane Helices 2 and 7 during Angiotensin AT_1 Receptor Activation

Gregory V. Nikiforovich[1,*], Meng Zhang[2], Qing Yang[2], Gowraganahalli Jagadeesh[2], Hao-Chia Chen[2], László Hunyady[3], Garland R. Marshall[1] and Kevin J. Catt[2]

[1]Department of Biochemistry and Molecular Biophysics, Washington University Medical School, St Louis, MO 63110, USA
[2]Endocrinology and Reproduction Research Branch, National Institute of Child Health and Human Development, National Institutes of Health, Bethesda, MD 20892-4510, USA
[3]Department of Physiology, Semmelweis University, Faculty of Medicine, H-1088 Budapest, Hungary
**Corresponding author: Gregory V. Nikiforovich, gregory@ccb.wustl.edu*

Site-directed mutagenesis studies and independent molecular modeling studies were combined to investigate the network of inter-residue interactions within the transmembrane region of the angiotensin AT_{1a} receptor. Site-directed mutagenesis was focused on residues Tyr292, Asn294, Asn295, and Asn298 in transmembrane helix 7, and the conserved Asp74 in helix 2 and other polar residues. Functional interactions between pairs of residues were evaluated by determining the effects of single and double-reciprocal mutations on agonist-induced AT_{1a} receptor activation. Replacement of Tyr292 by aspartate in helix 7 abolished radioligand binding to both Y292D and D74Y/Y292D mutant receptors. Reciprocal mutations of Asp74/Asn294, Ser115/Asn294, Ser252/Asn294, and Asn298/Sen115 caused additive impairment of function, suggesting that these pairs of residues make independent contributions to AT_{1a} receptor activation. In contrast, mutations of the Asp74/Tyr298 pair revealed that the D74N/N298D reciprocal mutation substantially increased the impaired inositol phosphate responses of the D74N and N298D receptors. Extensive molecular modeling yielded 3D models of the TM region of the AT_1 receptor and the mutants as well as of their complexes with angiotensin II, which were used to rationalize the possible reasons of impairing of function of some mutants. These data indicate that Asp74 and Asn298 are not optimally positioned for direct strong interaction in the resting conformation of the AT_{1a} receptor. Balance of interactions between residues in helix 2 (as D74) and helix 7 (as N294, N295 and N298) in the AT_1 receptors, however, has a crucial role both in determining their functional activity and levels of their expression.

Keywords: angiotensin receptor type 1; G protein-coupled receptors; molecular modeling; site- directed mutagenesis

Received 6 October 2006, revised 24 October 2006 and accepted for publication 25 October 2006

The octapeptide hormone, angiotensin II (Ang II; Asp[1]-Arg[2]-Val[3]-Tyr[4]-Ile/Val[5]-His[6]-Pro[7]-Phe[8]), is the major effector molecule of the renin-angiotensin system. Ang II acts as a crucial regulator in the maintenance of electrolyte and cardiovascular homeostasis by binding to specific cell surface receptors in its numerous target tissues. Pharmacologic and molecular biologic studies have identified two major Ang II receptor subtypes (1,2) termed AT_1 and AT_2 receptors, both of which are heptahelical transmembrane (TM) molecules that belong to the superfamily of G-protein-coupled receptors (GPCRs). To date, the known physiologic actions of Ang II appear to be mediated by the AT_1 receptor. Agonist binding to the AT_1 receptor is believed to induce a conformational change in the receptor molecule that is transmitted to the intracellular loops by the TM helices (3,4) and serves as an initial step for signal transduction (5–7).

Despite the great structural diversity in size and chemical composition of their activating ligands, all GPCRs share a common molecular architecture of seven TM α-helical domains that are linked by alternating extracellular and intracellular loops. So far, the 3D structure for only one GPCR, the photoreceptor rhodopsin, has been revealed at high resolution by X-ray crystallography (8–11) corresponding to its dark-adapted resting state. The 3D structure of the TM region of rhodopsin in the activated state was deduced from the experimental data of site-directed spin labeling (see Ref. 12); this structure is in good agreement with the results of independent energy calculations (13). The X-ray structure of rhodopsin has been used as a template for building 3D structures of other rhodopsin-like GPCRs, such as AT_1, in their inactive states [see, e.g. a minireview (14)]. The aim of the present study was to combine data on the 3D structure of the TM region of the AT_1 receptor independently obtained by molecular modeling and the results of the site-directed mutagenesis involving conserved residues in TM helices 2 and 7.

Specifically, several conserved residues on the polar surface of TM7, including Tyr292, Asn294, Asn298, and Tyr302, have been shown to be important for the agonist-induced conformational changes that initiate signal transduction from the AT_1 receptor (15–18).

Mutation of these residues causes significant impairment of the receptor's ability to couple to G proteins and activate inositol phosphate production (16,17,19,20). Also, the highly conserved aspartic acid residue (Asp74 in TM2 of the AT_1 receptor) is a major determinant of agonist-induced activation in many GPCRs, including the AT_1 receptor (19,20), where it was suggested to interact with Tyr292 or Asn295 in TM7 (15,21,22).

In the present study, we performed molecular modeling of the AT_1 receptor and its complex with Ang II, which elucidated various possibilities of residue–residue interactions involving the side chain of Asp74. Independently, site-directed mutagenesis was utilized to identify possible interhelical side chain interactions of Tyr292, Asn294, and Asn298 with Asp74 or other adjacent polar residues during receptor activation. Tyr292, Asn294, and Asn298 were substituted with their possible counterpart amino acids, and the latter were replaced with tyrosine or asparagine, respectively. To obtain gain-of-function evidence for interhelical interactions during AT_1 receptor activation, the ability of double mutant amino acids (in which tested pairs of amino acids were reversed) to rescue the impaired activation of the single mutant receptors was investigated.

Experimental Procedures

Materials

Inositol-free DMEM, FBS, and antibiotic solutions were from Biofluids (Rockville, MD, USA). Ang II was from Sigma Chemical Company (St Louis, MO, USA). ^{125}I-Ang II and ^{125}I-[Sar^1, Ile^8]Ang II were from Covance Laboratories (Vienna, VA, USA) or DuPont New England Nuclear (Boston, MA, USA). *myo*-[2-^{3}H]Inositol was from Amersham (Arlington Heights, IL, USA). OpitMEM and LipofectAMINE were from Life Technologies (Gaithersburg, MD, USA). Losartan was a gift from Dr P. C. Wong (DuPont, Wilmington, DE, USA).

Molecular modeling

The general procedure for building the TM bundle of the AT_1 receptor was essentially the same as described previously (23,24). First, TM helical fragments have been located in the sequence of the rat AT_1 receptor by sequence homology to the rhodopsin helices found by the CLUSTAL W procedure (http://ca.expasy.org/tools). The TM helices were thus determined as follows: TM1, F28-V41-Y54 (the first, middle and last residue, respectively); TM2, A63-C76-M90; TM3, H99-A114-I130; TM4, M142-W153-V164; TM5, I193-L205-L217; TM6, R234-F249-L265; and TM7, T282-Y292-Y302. The helical fragments were then assembled in a TM helical bundle for the AT_1 receptor and the mutants following the procedure of 'enhanced homology modeling', which consisted of (i) determining conformations of individual helices by independent energy minimization involving all dihedral angles starting from the values corresponding to the rhodopsin TM helices; (ii) superimposing the obtained conformations over the X-ray structure of Rh according to sequence homology, and (iii) packing helices by finding the energetically best arrangement of the individual helices, in which dihedral angles of the backbone are 'frozen' in the values obtained earlier. In fact, packing consisted of minimization of the sum of all intrahelical and interhelical interatomic energies in the multidimensional space of parameters that included the $6 \times 7 = 42$ 'global' parameters (those related to movements of individual helices as rigid bodies, namely, translations along the co-ordinate axes *X*, *Y*, *Z* and rotations around these axes T*x*, T*y*, and T*z*) and the 'local' parameters [the dihedral angles of the side chains for all helices; the starting values of those angles were optimized prior to energy minimization by an algorithm described earlier (25); see also Ref. (24)].

The co-ordinate system for the global parameters was selected as follows: the long axial *X* co-ordinate axis for each TM helix (TM1–TM7) has been directed from the first to the last C^{α}-atom; the *Y* axis was perpendicular to *X* and went through C^{α}-atom of the 'middle' residue of each helix; and the *Z* axis was built perpendicular to *X* and *Y* to maintain the right-handed co-ordinate system. For the complex of the AT_1 receptor with Ang II, the 'receptor-bound' conformation of AII deduced by us earlier has been docked to the developed 3D model of TM helical bundle of the AT_1 receptor starting from the $6 \times 8 = 48$ global parameters employed in the previous study (23). All energy calculations were performed using the ECEPP/2 force field with rigid valence geometry (26,27). Only *trans*-conformations of Pro residues were considered, and residues of Arg, Lys, Glu, and Asp were present as charged species. Each single run of energy minimization with energy convergence criterion of 1 kcal/mol required *ca.* 6–8 h on a single PC node of 2.8 GHz.

Mutagenesis and transient expression of mutant rat AT_1 receptors

The rat AT_1 receptor cDNA was subcloned into the mammalian expression vector, pcDNAI/Amp (Invitrogen, San Diego, CA, USA) as previously described (20). Mutant receptors were created using the Mutagene kit (Bio-Rad, Hercules, CA, USA) and mutated sequences were verified by dideoxy sequencing using Sequenase II (Amersham, Arlington Heights, IL, USA). COS-7 cells were seeded at 5×10^4 cells/well in 24-well culture plates and cultured in DMEM containing 10% (v/v) FBS, 100 IU/mL penicillin, and 100 μg/mL streptomycin (COS-7 medium) for 3 days. Transfection was performed with 0.5 mL of OptiMEM containing 8 μg/mL of LipofectAMINE and the required amount of DNA (usually 2 μg/mL) for 6 h at 37 °C. After replacement of fresh COS-7 medium the cells were cultured for a further 2 days prior to use.

[Sar^1,Ile^8]Ang II binding to intact cells

To determine the expression level and structural integrity of the mutant receptors, the number of Ang II-binding sites was determined by incubating the transfected cells with ^{125}I-[Sar^1,Ile^8]Ang II (0.05–0.1 μCi/sample) and increasing concentrations of unlabeled [Sar^1,Ile^8]Ang II in Medium 199 (HEPES) for 6 h at 4 °C. The cells were washed twice with ice-cold Dulbecco's phosphate-buffered saline and their associated radioactivity was measured by γ-spectrometry after solubilization with 0.5 M NaOH/0.05% SDS. The displacement curves were analyzed with the Ligand computer program using a one-site model (28).

Binding to COS-7 cell membranes

Forty-eight hours after transfection the cells were washed and scraped into 1.5 mL ice-cold 10 mM Tris–HCl (pH 7.4), 1 mM EDTA, then lysed by freezing and thawing. Crude membranes were prepared by centrifuging the samples at 16 000 × *g*. The pellet was resuspended in binding buffer (containing 100 mM NaCl, 5 mM $MgCl_2$, and 20 mM Tris–HCl, pH 7.4) and the protein content was determined. Binding assays were performed at 25 °C in 0.2 mL binding buffer supplemented with 2 g/L bovine serum albumin (BSA). Saturation binding experiments with ^{125}I-Ang II or ^{125}I-[Sar^1, Ile^8]Ang II were performed by adding increasing concentrations of the respective radioligand (up to 2 nM) to 15–30 μg of crude membranes. In displacement studies, each sample contained 0.05–0.1 μCi ^{125}I-Ang II or ^{125}I-[Sar^1,Ile^8]Ang II, 15–30 μg crude membranes, and the indicated concentrations of unlabeled ligand. After 90-min incubation at 25 °C, the unbound tracer was removed by rapid filtration and the bound radioactivity was measured by γ-spectrometry.

Inositol phosphate measurements

Transfected COS-7 cells in 24-well plates were labeled by 24-h incubation in inositol-free DMEM containing 0.1% (w/v) BSA, 2.5% (v/v) FBS, antibiotics, and 20 μCi/mL *myo*-[2-^{3}H]inositol. After washing and preincubation with 10 mM LiCl for 30 min, 1 μM Ang II was added for a further 20 min and incubations were stopped with perchloric acid. Inositol phosphates were extracted as described (16) and applied to Bio-Rad AG 1-X8 columns (Hercules, CA, USA). After washing three times with water and twice with 0.2 M ammonium formate, the combined inositol bisphosphate ($InsP_2$) + inositol trisphosphate ($InsP_3$) fractions were eluted with 1 M ammonium formate in 0.1 M formic acid, and radioactivities were determined by liquid scintillation counting. At the expression levels used in this study, there was a linear relationship between cell surface receptor expression and the magnitude of agonist-stimulated inositol phosphate production (17).

Results

Molecular modeling

AT_1 receptor

Initial building of the 3D model of the TM bundle of the AT_1 receptor was performed in accordance with structural homology to the X-ray structure of rhodopsin (the PDB entry 1F88, chain A) as outlined in Experimental Procedures; the procedure was quite similar to that described by us previously (23,24). This initial model differed from the X-ray structure of rhodopsin by the RMS value of 2.46 Å (C^α-atoms only). As our study was aimed at elucidation of possible interactions between residues in TM helices TM2 (as Asp74) and TM7 (as Tyr292, Asn294, and Asn298), we performed extensive configurational sampling of the TM bundle in the vicinity of the 'rhodopsin' configuration by rotating TM2 and TM7 along the long axes T*x*s on the grid of ΔT_2, ΔT_7 with the step of 10°. Sampling was started from the reference point of $\Delta T_2 = 0°$, $\Delta T_7 = 0°$ (the rhodopsin configuration) and covered most of the points on the grid of ΔT_2 from −20° to 40° and ΔT_7 from −20° to 20°. Totally, 25–30 configurations of the TM bundle were subjected to energy minimization.

Our energy calculations showed that the single configuration emerged as a clear local energy minimum for the TM bundle of AT_1 receptor. This configuration differed from the rhodopsin configuration by the slight deviations in parameters (the 'rhodopsin-like' configuration, $\Delta T_2 = 30°$, $\Delta T_7 = 10°$). This particular configuration was of distinctly lower relative energy (up to 20 kcal/mol) compared with the rhodopsin configuration. One can see that in this 3D structure the side chain of Asp74 is surrounded by three asparagine residues, namely Asn46 in TM1, Asn111 in TM3, and Asn295 in TM7 (see Figure 1). The side chains of asparagines bear the β-NH_2 and β-CO groups, both of which can be involved in hydrogen bonding and/or favorable electrostatic interactions with Asp74. The β-amide group of Asn298 is also oriented toward Asp74, though interaction between these two residues is weaker than those between Asn111 and Asn295 and Asp74. The spatial position of the Asn295 side chain is additionally stabilized by favorable interaction between the β-amide group of Asn295 and its own backbone carbonyl. Other significant inter-residue interactions highlighted in Figure 1 are the hydrogen bonding of the Ser115 hydroxyl to the α-carbonyl of Asn111; the close contact between the ε-amino group of Lys199 and the hydroxyl of Ser109; the favorable interaction between the β-carbonyl of Asn294 and the hydroxyl of Ser252; and close contact between the Asn200 and Gln257 side chains.

Complex of AT_1 and Ang II

Further, the initial 3D model of the complex of AT_1 receptor and Ang II was built according to Experimental Procedures based on the 3D model developed by us previously (23). The same procedure of configurational sampling by rotating TM2 and TM7 along the long axes in the vicinity of the rhodopsin configuration was performed for the AT_1 receptor + Ang II complex. The clear local energy minimum discovered in this case corresponded to the rhodopsin configuration ($\Delta T_2 = 0°$, $\Delta T_7 = 0°$). It can be assumed, therefore, that the TM bundle of AT_1 receptor may undergo slight configurational changes upon initial binding of Ang II.

The configuration of the complex is illustrated in Figure 1B. Spatial positions of the side chains of the residues discussed above are somewhat different from those in the AT_1 receptor without ligand. With the new α-carboxyl group of Phe^8 in Ang II introduced, the β-amide group of Asn111 interacts with both the α-carboxyl group of Phe^8 and the β-carboxyl of Asp74. The side chain of Asn295 may still be in close interaction with Asp74. Also, the spatial position of the side chain of Phe^8 of Ang II is stabilized by a 'sandwich-like' interaction with the side chain of His256. In addition, the β-carboxyl of Asp74 also interacts with the β-amide group of Asn46. It is noteworthy that a delicate balance exists in the entire system of these interactions. For instance, according to calculations the Asn295 side chain may change its spatial position to interact with the new α-carboxyl group, which weakens its interaction with the β-carboxyl of Asp74. As a result, the α-carboxyl group of Phe^8 in AII becomes co-ordinated by favorable interactions with both β-amide groups of Asn111 and Asn295.

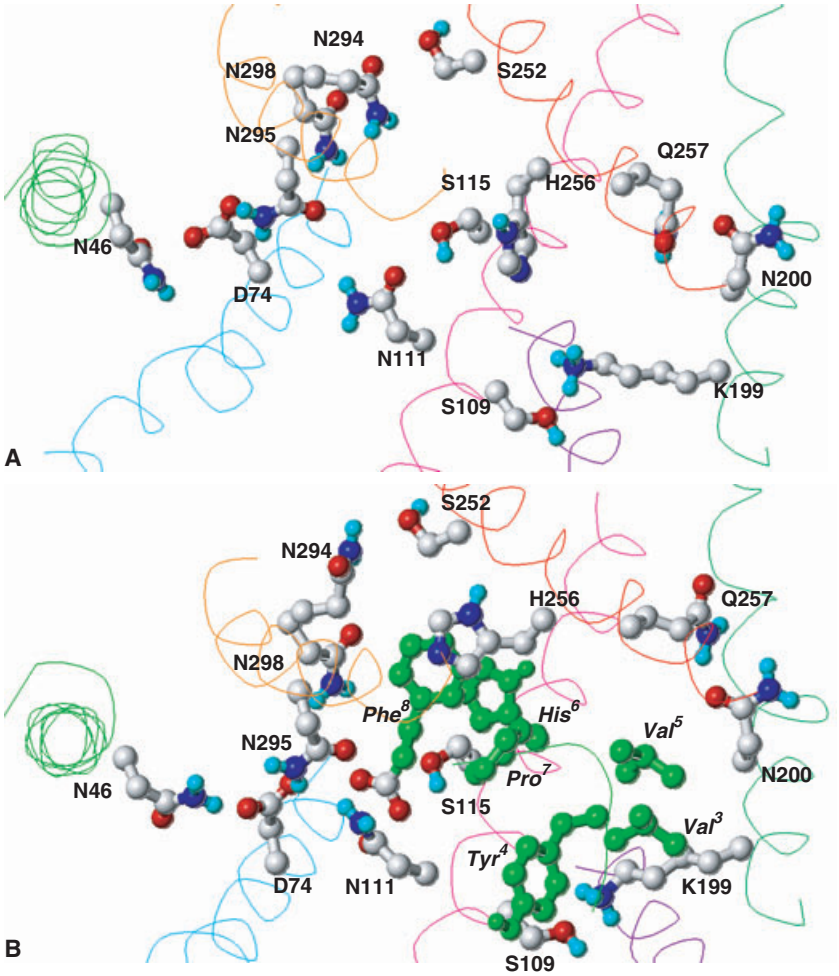

Figure 1: Sketches of 3D models of the TM region of the AT_1 receptor (A) and the receptor–Ang II complex (B). TM helices are shown as one-line ribbons in the following colors: TM1 in green, TM2 in cyan, TM3 in magenta, TM4 in purple, TM5 in green-blue, TM6 in red, and TM7 in orange; the trace of Ang II in panel B is shown in green. Both views are from the extracellular side normal to the membrane. Side chains of the discussed residues (including C^{α}-atoms) are shown as ball-and-stick models; side chains of Val^3, Tyr^4, Val^5, His^6, Pro^7, and Phe^8 are shown in panel B in green, except the C-terminal carboxyl of Ang II.

Mutant AT_1 receptors

Molecular modeling was also performed for a variety of AT_1 receptor mutants that were experimentally studied by site-directed mutagenesis either in this report (such as S115N, N294S, D74N, N294D, D74N/N298D, S252N, N298S, N298D, and Y292D) or in related studies from this [D74N (20), N294A, N295A (16) and N298A (17)] and other laboratories [D74E (19) and N298A (18)]. For all mutants, energy calculations were performed for two configurations, the rhodopsin one with $\Delta T_2 = 0°$, $\Delta T_7 = 0°$ and the rhodopsin-like configuration with $\Delta T_2 = 30°$, $\Delta T_7 = 10°$ for two cases, namely for mutants with and without Ang II. Rhodopsin-like configurations were always those with lower energy for mutants without Ang II (differences in relative energies up to 40 kcal/mol) with the only exception being the poorly expressed N298D (see Table 1). In contrast, for mutants complexed with Ang II the energies of the rhodopsin configurations were always lower than those of the rhodopsin-like ones (with differences up to 50 kcal/mol).

Finally, energy calculations for the wild-type (WT) AT_1 receptor and the mutants were repeated with some modifications of the employed ECEPP force field; first, electrostatic interactions were eliminated, and secondly, an additional cut-off for the non-bonded atomic interactions (for atom-atomic distances <8 Å) was introduced. As in the original calculations, the relative energies of the rhodopsin versus rhodopsin-like configurations were higher for the TM bundles without Ang II, and lower for the AT_1 receptor + Ang II complexes in both cases. These results strongly suggest that the differences in relative energies were not due to some specific terms of the force fields used in our calculations.

Biologic data

[Sar^1,Ile^8]Ang II-binding properties of mutant AT_1 receptors

A series of substitution and reciprocal mutant AT_1 receptors was constructed to determine the dependence of AT_1 receptor activation on the interaction of the functionally most important residues in TM7 with adjacent residues based on this model, or suggested to interact in previous studies. Most mutations had no major effect on the affinity of the receptor for the peptide antagonist, [Sar^1,Ile^8]Ang II (Table 1), indicating that they did not disturb the structure and folding of the expressed receptors. To test the possibility of interaction between Asp74 and Tyr292, the effect of reversing these residues was examined. The presence of a negatively charged aspartic acid residue in position 292 was not tolerated, however, and no detectable binding of [Sar^1,Ile^8]Ang II to the Y292D point mutant or the D74Y-Y292D reverse mutant AT_1 receptors was observed. The other mutant AT_1 receptors displayed considerable variation in their

Table 1: Binding parameters of mutant AT_1 receptors for ^{125}I-[Sar^1,Ile^8]Ang II

Receptor	K_d (nM)	Binding sites (% of wild type)
Wild type	1.6 ± 0.1	100
S115N	1.7 ± 0.4	130 ± 32
N294S	1.3 ± 0.2	140 ± 44
S115N-N294S	1.6 ± 0.1	180 ± 40
D74N	1.7 ± 0.1	102 ± 20
N294D	1.3 ± 0.2	23 ± 5
D74N-N294D	1.5 ± 0.2	48 ± 9
S252N	2.3 ± 0.2	14 ± 3
S252N-N294S	2.4 ± 0.4	17 ± 4
N298S	1.7 ± 0.1	47 ± 3
S115N-N298S	1.6 ± 0.1	64 ± 3
D74N-N298S	2.5 ± 0.2	111 ± 2
N298D	1.3 ± 0.2	6 ± 1
D74N-N298D	1.6 ± 0.1	47 ± 2
D74Y	2.3 ± 0.5	23 ± 5
Y292D	Not detectable	Not detectable
D74Y-Y292D	Not detectable	Not detectable

All K_d and B_{max} values were calculated using the LIGAND program. The numbers of expressed binding sites are shown as a percentage of the binding sites of the wild-type AT_1 receptors measured in the same experiment. The expression level of the wild-type AT_1 receptor was 2.54 ± 0.53 pmol/mg protein. The data are expressed as mean ± SEM of three independent experiments each performed in duplicate.

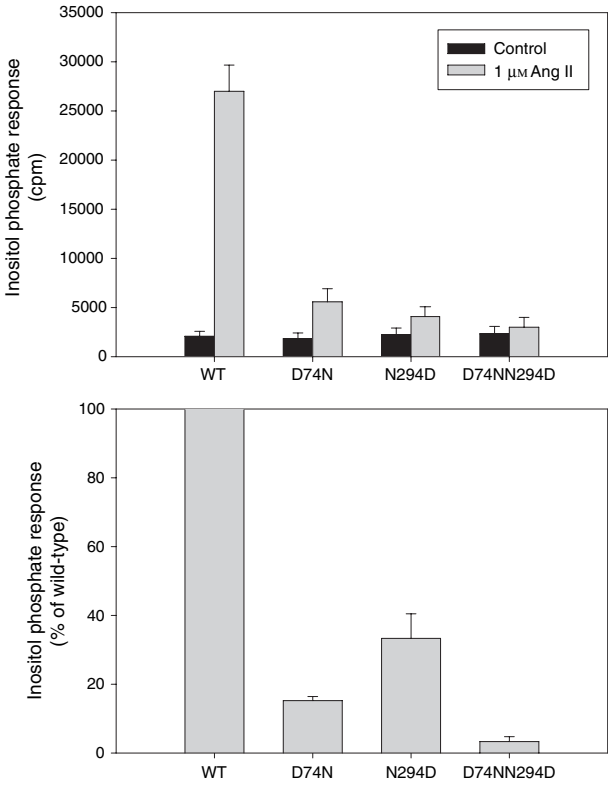

Figure 2: Inositol phosphate responses of Asp74/Asn294 mutant AT_1 receptors. [^{3}H]Inositol-labeled COS-7 cells expressing the indicated receptors were preincubated with 10 mM LiCl for 30 min prior to addition of 1 μM Ang II for a further 20 min. In this and subsequent figures, Ang II-stimulated [^{3}H]inositol phosphates were measured as described in Experimental Procedures. (A) Combined radioactivities of $InsP_2$/$InsP_3$ production for each mutant; (B) inositol phosphate responses data were normalized to an equal number of binding sites for each mutant, and expressed as a percentage of the wild-type response. The data represent mean ± SEM from three independent experiments each performed in duplicate.

expression levels compared with the WT receptor, while the expression level of the N298D mutant receptors was also substantially reduced (Table 1).

Inositol phosphate responses of mutant AT_1 receptors

The abilities of the single and reciprocal double mutant receptors to induce inositol phosphate signal generation were evaluated in transfected COS-7 cells prelabeled with [^{3}H]inositol for 24 h. The radioactivities of combined $InsP_2$ + $InsP_3$ fractions were measured after stimulation of the cells with maximally effective concentration of Ang II (1 μM) for 20 min in the presence of 10 mM LiCl.

The possible interactions of Asp74 in TM2 with Ser115 in TM3, and Ser252 in TM6 during receptor activation were also tested. In accordance with previous studies (19,20), the D74N mutant receptor had markedly impaired inositol phosphate responses (Figure 2). The N294D mutant receptor exhibited similarly reduced Ang II-induced inositol phosphate responses, as well as relatively low expression. A considerable decrease in the amplitude of the inositol phosphate responses of the N294D mutant was evident after normalization of the responses to the expression level of the receptor (Figure 2, lower panel), consistent with the impaired G-protein coupling of this receptor (16). The (D74N/N294D) reciprocal mutation did not restore the impaired signaling of the individual mutants, and its inhibitory effect on inositol phosphate generation appeared to be additive.

To test the possible interaction of Asn294 with Ser115 or Ser294, an N294S mutant AT_1 receptor was created. Substitution of Asn294 with serine attenuated the agonist-induced inositol phosphate response (Figures 3 and 4) but did not change the expression level of the receptor (Table 1). Substitution of Ser115 with asparagine also reduced the inositol phosphate signal. The N294S/S115N reciprocal mutation did not rescue the signaling response of the receptor, but instead decreased it to below those of the individual mutant receptors (Figure 3). Substitution of Ser252 with asparagine also impaired signal generation by the receptor, but this effect was largely due to its reduced expression level (Figure 4). The N294S/S252N reciprocal mutation did not restore the impaired inositol phosphate signal generation of the N294S receptor (Figure 4), and also had a low expression level. These data argue against the roles of Asp74, Ser115, and Ser252 as counterparts of Asn294 in an intramolecular interaction during AT_1 receptor activation. However, the latter conclusion may be considered less reliable, as both S252N and N294S/S252N were poorly expressed.

The possible interactions of Asn298 with Ser115 or Asp74 during receptor activation were also evaluated. Asn298 is part of the

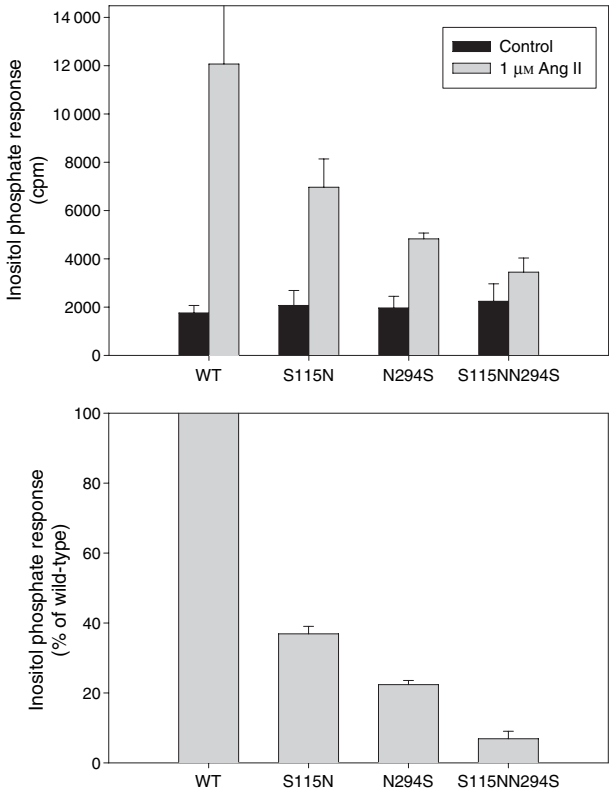

Figure 3: Inositol phosphate responses of Ser115/Asn294 mutant AT_1 receptors. Transfected COS-7 cells were prelabeled with [^{3}H]inositol, preincubated with 10 mM LiCl, and incubated in the absence (black bars) or presence (gray bars) of 1 μM Ang II. (A) Combined radioactivities of $InsP_2$ + $InsP_3$ fractions of each mutant; (B) inositol phosphate responses normalized to an equal number of expressed binding sites for each mutants and expressed as a percentage of wild-type response. The data represent mean ± SEM from three independent experiments each performed in duplicate.

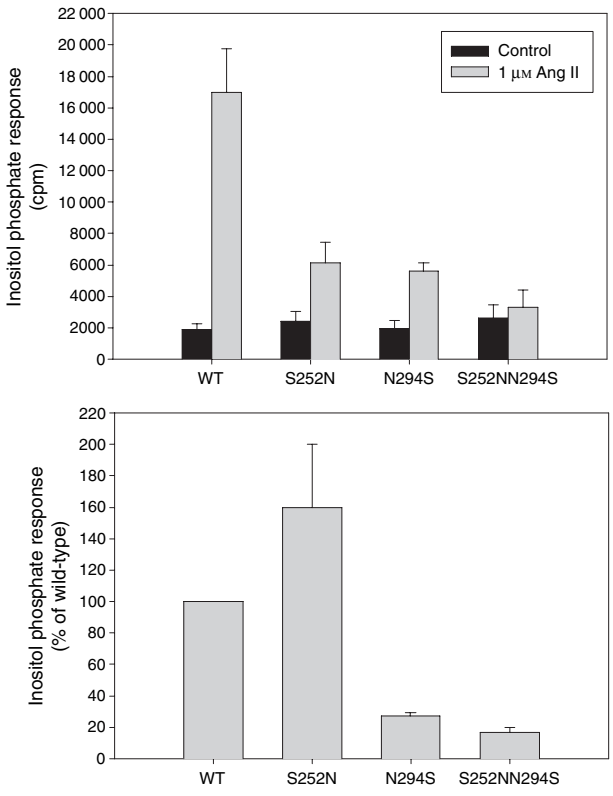

Figure 4: Inositol phosphate responses of S252/Asn294 mutant AT_1 receptors. [^{3}H]Inositol-labeled COS-7 cells expressing the indicated receptors were preincubated with 10 mM LiCl for 30 min prior to the addition of 1 μM Ang II for an additional 20 min. (A) Combined radioactivities of $InsP_2$ + $InsP_3$ fractions of each mutant; (B) inositol phosphate responses normalized to an equal number of expressed binding sites for each mutant and expressed as a percentage of the wild-type response. The data represent mean ± SEM from three independent experiments each performed in duplicate.

highly conserved $NPX_{2-3}Y$ sequence in most GPCRs, and has been proposed to interact with the highly conserved Asp residue in TM2, based on the effects of reversal of these amino acids in several GPCRs (29–33). Substitution of Ser115 with asparagine, or Asn298 with serine, moderately impaired inositol phosphate generation by the mutant receptors, but the effect of reciprocal mutations of Asn298–Ser115 appeared to be additive (Figure 5). Substitution of Asn298 with aspartic acid markedly reduced the expression level of the receptor (Table 1). In accordance with this finding, inositol phosphate generation by the N298D mutant was also diminished (Figure 6). The very low expression of the N298D receptor (6% of WT) prevented accurate normalization of the inositol phosphate responses in the lower panel of Figure 6. The D74N/N298D reciprocal mutation increased the expression of the receptor to almost 50% of the WT (Table 1), and substantially increased the agonist-induced inositol phosphate response above that of the D74N receptor (Figure 6). As a control for the enhancing effect of the N298D mutation, an N298S mutant receptor was created and was found to be well expressed. However, the D74N/N298S double mutation did not correct the impaired inositol phosphate responses of the D74N receptor (Figure 6), indicating that the positive effect of the D74N/N298D mutation on receptor function was specific for the aspartic acid substitution of Asn298.

Discussion

Validity of 3D models for TM region of AT_1 and its complex with Ang II

The 3D models of the TM region of the AT_1 receptor and the AT_1 receptor + Ang II complex suggested by molecular modeling in this study are largely similar, and the difference between them is primarily the small rotation of TM2. One can assume that in the absence of Ang II the AT_1 receptor exists in its resting state in the rhodopsin-like configuration, which undergoes slight changes upon binding Ang II by switching to the rhodopsin configuration. The latter, however, cannot be regarded as the 3D model of the TM bundle of the AT_1 receptor in the activated state, but rather as the initial 3D model of the AT_1 receptor + Ang II complex still in the resting state (the 'preactivated' state).

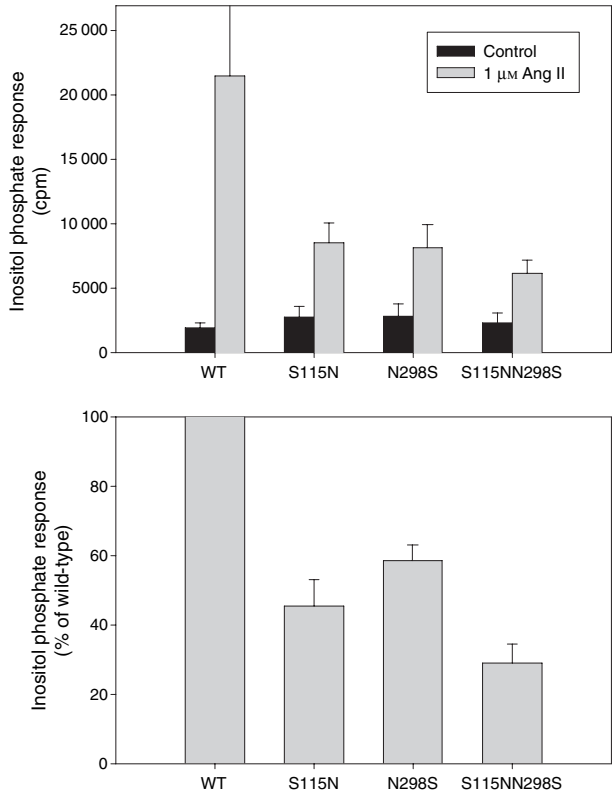

Figure 5: Inositol phosphate responses of Ser115/Asn298 mutant AT_1 receptors. [^{3}H]Inositol-labeled COS-7 cells expressing the indicated receptors were preincubated with 10 mM LiCl for 30 min prior to the addition of 1 μM Ang II for an additional 20 min. Ang II-stimulated [^{3}H]Inositol phosphates were measured as described in the Experimental Procedures. (A) Combined radioactivities of $InsP_2$ + $InsP_3$ fractions of each mutant; (B) inositol phosphate responses normalized to an equal number of expressed binding sites for each mutant and expressed as a percentage of wild-type response. The data represent mean ± SEM from three independent experiments each performed in duplicate.

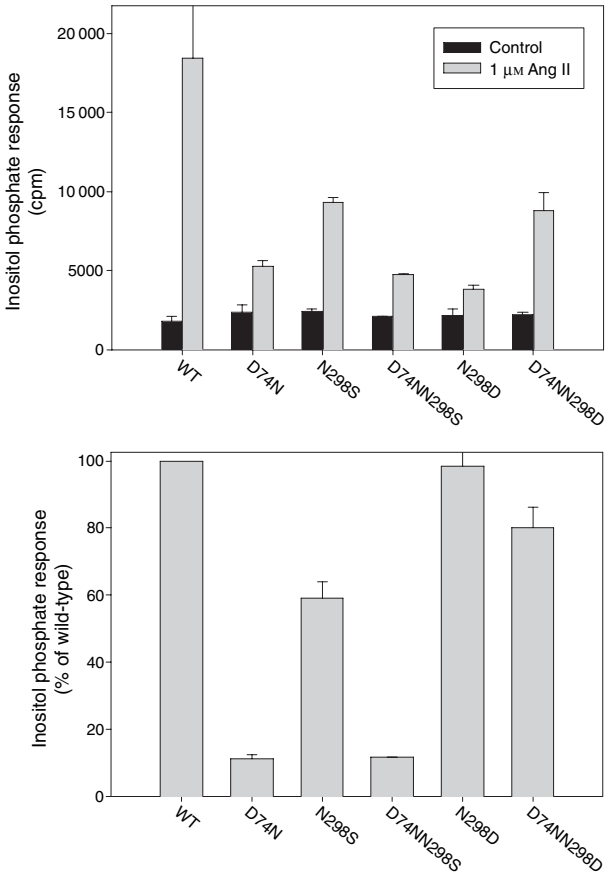

Figure 6: Inositol phosphate responses of Asp74/Asn298 mutant AT_1 receptors. [^{3}H]Inositol-labeled COS-7 cells expressing the indicated receptors were preincubated with 10 mM LiCl for 30 min prior to the addition of 1 μM Ang II for an additional 20 min. (A) Combined radioactivities of $InsP_2$ + $InsP_3$ fractions of each mutant; (B) inositol phosphate responses normalized to an equal number of expressed binding sites for each mutants (except N298D, where the binding sites were too low to normalize) and expressed as a percentage of the wild-type response. The data represent mean ± SEM from three independent experiments each performed in duplicate.

The 3D model of the AT_1 receptor–Ang II complex suggested in the present study is similar to the model developed and discussed by us previously (23), which has been shown to be in good agreement with most established data on site-directed mutagenesis of the AT_1 receptors. For instance, the model brings together Asn111 and Phe^8 (including the α-carboxyl), which are the two elements most crucial for initiating constitutive activity and triggering InsP production in the AT_1 receptor and Ang II, respectively. It also agrees with the observation that Asn295 may be replaced by a variety of amino acid residues without significant loss of function (16,34,35). In these cases, interactions of the β-amide group of Asn111 with the α-carboxyl group of Phe^8 compensate for the loss of interaction involving the β-amide group of Asn295. The pivotal role of the β-carbonyl of Asp74, as suggested by the model, is also consistent with the available data on site-directed mutagenesis. Thus, the D74N and D74E mutants exhibit markedly decreased functional activity [(19); see also the discussion below], and [Sar^1,Ile^8]Ang II almost completely loses affinity for the D74K mutant (36). The model also rationalizes the decreased affinity of the AT_1 receptor for Ang II-NH_2 when compared with Ang II (37), but does not support the proposed hydrogen bonding of the ε-amino group of Lys199 and the α-carboxyl group of Phe^8 (37). However, this interaction, in our view, is also contradicted by the data on comparable binding affinity of Ang II and Ang II-NH_2 (and [Sar^1]-Ang II and [Sar^1]-Ang II-NH_2) to the K199E receptor (38).

More recent and direct experimental data lend additional support for the model. For instance, extensive studies that employed photolabeled analogs of Ang II (39–42) applied the methionine scan of TM3, TM6, and TM7 of the AT_1 receptor determining residues L112, Y113, F249, W253, H256, T260, F293, N294, N295, C296, and L297 as those involved in binding pocket of Ang II [the Phe^8-labeled analogs of Ang II were used; (41)]. These results are very close to our model, which shows residues of AT_1 receptor directly interacting with Ang II as follows: Phe77 with

the α-carboxyl of Phe^8; Ser105 with Tyr^4; Asn111 with the α-carboxyl of Phe^8; Leu112 with Val^5; Asn200 with Val^5; Phe249 with Val^5; Trp253 with Val^5; His256 with His^6 and Phe^8; Thr260 with Val^3; Met284 with Asp^1; Asn294 with Phe^8; and Asn295 with Phe^8 and with the α-carboxyl of Phe^8 (direct contact was presumed when distances between at least one pair of atoms belonging to the side chains of AT_1 receptor and Ang II were <4 Å). In fact, the 3D model of the AT_1 receptor + Ang II complex proposed on the basis of the above experimental findings is highly compatible with our current model as well as that suggested earlier (23), as has been noted in a related publication (40). The main difference between the models is in assuming the extended conformation of Ang II in Refs (39–41), which appears to contradict the known high binding affinity of a variety of cyclic analogs of Ang II for the AT_1 receptor [see e.g. (43) and references therein].

Other 3D models of the AT_1 receptor + Ang II complex suggested by means of molecular modeling and based on the structure of bacteriorhodopsin, which is not a GPCR, have been previously discussed in detail (23). Two other rhodopsin-based models are currently available on the Internet and in the literature (44,45). The general spatial arrangements of TM helices in both of these are similar to our model, which is expected because all three models are based on the same X-ray structure of rhodopsin. Differences in the relative spatial positions of residues Asp74, Asn111, Asn294, Asn295, and Asn298 are, however, more significant. The first model places the side chain of Asp74 close to that of Asn46, but the side chains of Asn111, Asn295, and Asn298 are separated from it by *ca.* 6–8 Å (44). On the contrary, the second model presumes hydrogen bonding between the β-carboxyl of Asp74 and the β-amino groups of both Asn111 and Asn298 (45). Neither of the models suggests close contacts between His256 and Phe^8 of Ang II, which have been proposed to be important for receptor activation (37). The Ang II conformation employed in the first model resembles a somewhat distorted conformation used in our model [see also Ref. (44)]. However, the orientation of Ang II differs from our model in that the Tyr^4 residue of Ang II is most deeply inserted into the TM bundle, in contradiction with experimental data that show deep immersion of Phe^8, but not Tyr^4, into the TM bundle (39–41). The second model features the Ang II conformation directly converted to 3D from 2D structure using the CHEM3D program [see Ref. (45)]; as a result, the Tyr^4 residue acquired values of the backbone dihedral angles ϕ and ψ that are inconsistent with any low-energy conformation of the L-amino acid residue (the positive ϕ combined with the negative ψ). On the other hand, this model, like ours, contains the close contact between the ε-amino group of Lys199 and the hydroxyl of Ser109. The ε-amino group of Lys199 is also involved in the salt bridge with the α-carboxyl of Phe^8 in both models.

Combining the data of modeling and site-directed mutagenesis

We have applied our 3D models of the AT_1 receptor and the mutants to interpret the data of site-directed mutagenesis obtained in this study. The commonly accepted assumption is that the effects of mutations at different positions of a protein molecule should be additive if their actions are independent (46). In contrast, substitution of interacting residues should not result in additive impairment of function, and reversal of an interacting pair of amino acids may restore the impaired function. The experimental findings of our study show that the impairment of Ang II-induced signal generation was additive for the reversal mutants of the Asn294/Ser115, Asn298/Asp74, and Asn298/Ser115 amino acid pairs. Based on these data and on the above assumption, direct interactions between these amino acid pairs are unlikely to contribute to the stabilization of the active conformation of the receptor. The data on the Asn294/Ser252 amino acid pair should be regarded as less reliable for interpretation purposes, as mutants S252N and S252N/N294S were relatively poorly expressed (see Table 1).

Our 3D models of the complexes of the AT_1 receptors and Ang II in the resting state confirm that contributions of Asn294 and Ser115 or Asn298 and Ser115 to receptor activation are independent. Those residues are located far apart from each other (see Figure 1) and their interactions are unlikely in any probable active state of the receptor, which may differ from the resting state by rotations of TM helices around their long axes, as suggested in several studies of the AT_1 receptor (47–50). However, Asp74 and Asn298 are closer to each other, and, in some cases may be involved in general interactions between TM2 and TM7. This view is also in agreement with experimental data obtained by the SCAM technique, which suggested rotation of TM2 in the process of constitutive activation due to the N111G mutation, accompanied by rotation of TM7 (47,48). Similarly, constitutive activation in N111G was suggested to be associated with movement of TM7 in the experimental SCAM study (49).

Mutations of the Asp74/Asn298 pair caused a pattern of changes that differed from those of all other tested amino acid pairs. The individual D74N and N298S mutant receptors showed impaired inositol phosphate signaling, but the effects of these mutations were not additive. The magnitude of the inositol phosphate response was similar for the D74N mutant receptor and the D74N/N298S double mutant receptor. The reciprocal D74N/N298D mutation rescued the impaired inositol phosphate signaling capacity of the D74N mutant AT_1 receptor. These findings suggest that the conserved Asp74 and Asn298 residues could participate in an intramolecular interaction that stabilizes the active conformation of the receptor.

The asparagine residue in position 294 was also found to be important for manifesting functional activity; specifically, N294D was poorly expressed (see Table 1), and N294S and N294A retained only *ca.* 20–30% and *ca.* 15% of IP production of that of WT, respectively [see Figures 3 and 4 and Ref. (16)]. In these cases, the data from molecular modeling do not provide any clear indications about possible changes in interhelical interactions. However, the spatial orientation of the important Ser252 side chain in TM6 is changed in N294A and N294S compared with WT, where it can be involved in favorable interaction with Asn294 (see Figure 1).

Balance of residue–residue interactions in the AT_1 + Ang II complex

Although the 3D structure of the activated state of the AT_1 receptor is not yet known, it is reasonable to assume that transition from the resting to the activated state could be hindered by intramolecular interac-

tions stabilizing the former over the latter state. In this regard, comparison of the 3D models of the complexes of the AT_1 receptor mutants and Ang II with that of the WT shows that the balance of interactions between residues in positions 74, 111, 295, 298, and the α-carboxyl of Phe^8 in Ang II, may indeed change in the suggested way. For instance, in the D74N mutant (*ca.* 15% of IP production compared with that of the WT, see Figure 2), interaction between Asn74 and the α-carboxyl of Phe^8 was more favorable than in the WT (the change in interhelical energy associated with this mutation was *ca.* −14.7 kcal/mol), which may hinder possible rotations of the TM2 helix. Similarly, for the totally impaired D74E mutant (19), the longer side chain of Glu74 allows more favorable interaction with Asn298 with only slight weakening of interaction with the α-carboxyl of Phe^8 (total change in the related interhelical energy was *ca.* –5.2 kcal/mol), which may limit potential rotations of both TM2 and TM7. However, in D74N/N298D the stronger interactions between Asn74 and the α-carboxyl of Phe^8 (as in D74N) are compensated by greater electrostatic repulsion between Asp298 and the α-carboxyl of Phe^8 (as in N298D, see above). At the same time, elimination of the side chain in position 295 does not significantly affect functionality [N295A, *ca.* 65% of IP production of WT (16)], as the absence of interactions between Asn295 and Asp74 or the α-carboxyl of Phe^8 leads to strengthening of the interactions between Asn111 and the α-carboxyl of Phe^8. On the other hand, replacements of the asparagine side chain in position 298 by alanine [N298A, *ca.* 40% of IP production of WT (17)] or serine (*ca.* 60%, Figures 5 and 6) causes rather small changes in interhelical interactions in WT. In the double mutants with modifications in position 74, one can expect more profound changes accompanied by lowering of InsP production (as in D74N/N298S, *ca.* 10%, Figure 6).

Significance of interaction between the conserved Asp and Asn residues

Residues Asp74 in TM2 and Asn298 in the $NPX_{2-3}Y$ sequence of TM7 are highly conserved residues in most GPCRs. Several studies investigated mutations of these conserved residues in various receptors introducing single D↔N and N↔D mutations as well as the reciprocal N↔D/D↔N mutation that in most cases has restored functional activity impaired by the D↔N mutation (29–32,51). Earlier studies considered the possibility of direct hydrogen bonding between the two residues upon activation without involvement of other residues [e.g. for the gonadotropin-releasing hormone receptor, GnRH-R (32), and the human serotonin 5-HT_{2A} receptor (30)]. This was supported by the fact that amino acids corresponding to Asp74 and Asn298 are naturally reversed in some mammalian receptors of the GnRH-R. Interestingly, while reciprocal mutation of these residues partially restored GnRH binding in the mouse GnRH-R (32), no restoration was observed in the same mutants of the rat GnRH-R (33). Subsequent studies suggested the existence of a more extended hydrogen bond network between the conserved residues that correspond to Asn46, Asp74, Asn298, and Tyr302 in the AT_1 receptor in the mouse thyrotropin-releasing hormone receptor (31) and the human tachykinin NK_2 receptor (29). A recent study on the human thyrotropin receptor (51) described a system of interactions between the two residues that involves residues in TM6 and the internal water molecules. Thus, our data that emphasize the complex nature of interactions between TM2 and TM7 in the AT_1 receptor upon activation are consistent with observations by other authors.

In conclusion, our findings yielded 3D models of the TM region of AT_1 and AT_1 + Ang II that are in good agreement with the available experimental data. Comparison of the models showed slight but important differences in rotations of TM helices 2 and 7 between the initial resting state of AT_1 (without Ang II) and the 'preactivated' state (with Ang II bound to AT_1). This observation was employed to rationalize the results of site-directed mutagenesis that involve mutations of residues in TM2 (D74), TM3 (S115), TM6 (S252), and TM7 (Y292, N294, and N298). Although not all aspects of ligand binding and signal transduction were fully investigated by site-directed mutagenesis, the obtained experimental data, together with data on other receptors, indicate that an interaction between the conserved aspartic acid residue in TM2 and the asparagine residue of the conserved $NPX_{2-3}Y$ sequence in TM7 may have a general function in GPCR activation. However, according to the data of molecular modeling, in the AT_1 receptor this interaction is mediated by the balance of other interactions between residues in TM2 (D74) and TM7 (D294, D295, and D298). This suggests that, as residues corresponding to D294 and D295 in the AT_1 receptor are not conserved in other GPCRs belonging to the rhodopsin family, the molecular mechanisms determining the crucial interactions between TM2 and TM7 could differ significantly among individual receptors.

Acknowledgments

The excellent technical assistance of Yue Zheng is greatly appreciated. The authors are grateful to Dr S. S. Karnik for providing information on the 3D model of the AT_1 + Ang II complex prior to publication of Ref. 45. The work of L. H. was supported by the Hungarian Science Foundation (OTKA T-046445). G.V.N. and G.R.M. were partly supported by NIH grant GM 68460.

References

1. Timmermans P.B.M.W.M., Wong P.C., Chiu A.T., Herblin W.F., Benfield P., Carini D.J., Lee R.J., Wexler R.R., Saye J.A.M., Smith R.D. (1993) Angiotensin II receptors and angiotensin II receptor antagonists. Pharmacol Rev;45:205–251.
2. Inagami T. (1999) Molecular biology and signaling of angiotensin receptors: an overview. J Am Soc Nephrol;10 (Suppl. 11):S2–S7.
3. Hunyady L., Balla T., Catt K.J. (1996) The ligand binding site of the angiotensin AT_1 receptor trends. Pharmacol Sci;17:135–140.
4. Thomas W.G. (1999) Regulation of angiotensin II type 1 (AT_1) receptor function. Regul Pept;79:9–23.
5. Hunyady L., Catt K.J. (2006) Pleiotropic AT1 receptor signaling pathways mediating physiological and pathogenic actions of angiotensin II. Mol Endocrinol;20:953–970.
6. Griendling K.K., Lassègue B., Alexander R.W. (1996) Angiotensin receptors and their therapeutic implications. Annu Rev Pharmacol Toxicol;36:281–306.
7. Spät A., Hunyady L. (2004) Control of aldosterone secretion: a model for convergence in cellular signaling pathways. Physiol Rev;84:489–539.

8. Palczewski K., Kumasaka T., Hori T., Behnke C.A., Motoshima H., Fox B.A., Le Trong I., Teller D.C., Okada T., Stenkamp R.E., Yamamoto M., Miyano M. (2000) Crystal structure of rhodopsin: a G protein-coupled receptor. Science;289:739–745.
9. Teller D.C., Okada T., Behnke C.A., Palczewski K., Stenkamp R.E. (2001) Advances in determination of a high-resoultion three-dimensional structure of rhodopsin, a model of G-protein-coupled receptors (GPCRs). Biochemistry;40:7761–7772.
10. Okada T., Fujiyoshi Y., Silow M., Navarro J., Landau E.M., Shichida Y. (2002) Functional role of internal water molecules in rhodopsin revealed by X-ray crystallography. Proc Natl Acad Sci U S A;99:5982–5987.
11. Li J., Edwards P.C., Burghammer M., Villa C., Schertler G.F. (2004) Structure of bovine rhodopsin in a trigonal crystal form. J Mol Biol;343:1409–1438.
12. Hubbell W.L., Altenbach C., Khorana H.G. (2003) Rhodopsin structure, dynamics and activation. Adv Protein Chem;63:243–290.
13. Nikiforovich G.V., Marshall G.R. (2003) 3D model for meta-II rhodopsin, an activated G-protein-coupled receptor. Biochemistry;42:9110–9120.
14. Ballesteros J.A., Shi L., Javitch J.A. (2001) Structural mimicry in G protein-coupled receptors: implications of the high-resolution structure of rhodopsin for structure-function analysis of rhodopsin-like receptors. Mol Pharmacol;60:1–19.
15. Marie J., Maigret B., Joseph M.-P., Larguier R., Nouet S., Lombard C., Bonnafous J.-C. (1994) Tyr(292) in the seventh transmembrane domain of the AT_{1a} angiotensin II receptor is essential for its coupling to phospholipase C. J Biol Chem;269:20815–20818.
16. Hunyady L., Ji H., Jagadeesh G., Zhang M., Gaborik Z., Mihalik B., Catt K.J. (1998) Dependence of AT_1 angiotensin receptor function on adjacent asparagine residues in the seventh transmembrane helix. Mol Pharmacol;54:427–434.
17. Hunyady L., Bor M., Baukal A.J., Balla T., Catt K.J. (1995) Critical role of a conserved intramembrane tyrosine residue in angiotensin II receptor activation. J Biol Chem;270:16602–16609.
18. Laporte S.A., Servant G., Richard D.E., Escher E., Guillemette G., Leduc R. (1996) The tyrosine within the NPXnY motif of the human angiotensin II type 1 receptor is involved in mediating signal transduction but is not essential for internalization. Mol Pharmacol;49:89–95.
19. Bihoreau C., Monnot C., Davies E., Teutsch B., Bernstein K.E., Corvol P., Clauser E. (1993) Mutation of Asp ^{74} of the rat angiotensin-II receptor confers changes in antagonist affinities and abolishes G-protein coupling. Proc Natl Acad Sci U S A;90:5133–5137.
20. Hunyady L., Baukal A.J., Balla T., Catt K.J. (1994) Independence of type I angiotensin II receptor endocytosis from G protein coupling and signal transduction. J Biol Chem;269:24798–24804.
21. Joseph M.P., Maigret B., Bonnafous J.C., Marie J., Scheraga H.A. (1995) A computer modeling postulated mechanism for angiotensin II receptor activation. J Protein Chem;14:381–398.
22. Inoue Y., Nakamura N., Inagami T. (1997) A review of mutagenesis studies of angiotensin II type 1 receptor, the three-dimensional receptor model in search of the agonist and antagonist binding site and the hypothesis of a receptor activation mechanism. J Hypertens;15:703–714.
23. Nikiforovich G.V., Marshall G.R. (2001) 3D model for TM region of the AT-1 receptor in complex with angiotensin II independently validated by site-directed mutagenesis data. Biochem Biophys Res Commun;286:1204–1211.
24. Nikiforovich G.V., Mihalik B., Catt K.J., Marshall G.R. (2005) Molecular mechanisms of constitutive activity: mutations at position 111 of the angiotensin AT_1 receptor. J Pept Res;66:236–248.
25. Nikiforovich G.V., Hruby V.J., Prakash O., Gehrig C.A. (1991) Topographical requirements for delta-selective opioid peptides. Biopolymers;31:941–955.
26. Dunfield L.G., Burgess A.W., Scheraga H.A. (1978) Energy parameters in polypeptides: 8. Empirical potential energy algorithm for the conformational analysis of large molecules. J Phys Chem;82:2609–2616.
27. Nemethy G., Pottle M.S., Scheraga H.A. (1983) Energy parameters in polypeptides: 9. Updating of geometrical parameters, nonbonded interactions, and hydrogen bond interactions for the naturally occuring amino acids. J Phys Chem;87:1883–1887.
28. Munson P.J., Rodbard D. (1980) Ligand: a versatile computerized approach for characterization of ligand-binding systems. Anal Biochem;107:220–239.
29. Donnelly D., Maudsley S., Gent J.P., Moser R.N., Hurrell C.R., Findlay J.B. (1999) Conserved polar residues in the transmembrane domain of the human tachykinin NK2 receptor: functional roles and structural implications. Biochem J;339:55–61.
30. Sealfon S.C., Chi L., Ebersole B.J., Rodic V., Zhang D., Ballesteros J.A., Weinstein H. (1995) Related contribution of specific helix 2 and 7 residues to conformational activation of the serotonin 5-HT2A receptor. J Biol Chem;270:16683–16688.
31. Perlman J.H., Colson A.O., Wang W., Bence K., Osman R., Gershengorn M.C. (1997) Interactions between conserved residues in transmembrane helices 1, 2, and 7 of the thyrotropin-releasing hormone receptor. J Biol Chem;272:11937–11942.
32. Zhou W., Flanagan C., Ballesteros J.A., Konvicka K., Davidson J.S., Weinstein H., Millar R.P., Sealfon S.C. (1994) A reciprocal mutation supports helix 2 and helix 7 proximity in the gonadotropin-releasing hormone receptor. Mol Pharmacol;45:165–170.
33. Cook J.V., Faccenda E., Anderson L., Couper G.G., Eidne K.A., Taylor P.L. (1993) Effects of Asn87 and Asp318 mutations on ligand binding and signal transduction in the rat GnRH receptor. J Endocrinol;139:R1–4.
34. Feng Y.H., Miura S., Husain A., Karnik S.S. (1998) Mechanism of constitutive activation of the AT_1 receptor: influence of the size of the agonist switch binding residue Asn^{111}. Biochemistry;37:15791–15798.
35. Balmforth A.J., Lee A.J., Warburton P., Donnelly D., Ball S.G. (1997) The conformational change responsible for AT_1 receptor activation is dependent upon two juxtaposed asparagine residues on transmembrane helices III and VII. J Biol Chem;272:4245–4251.
36. Feng Y.H., Noda K., Saad Y., Liu X.P., Husain A., Karnik S.S. (1995) The docking of Arg^2 of angiotensin II with Asp^{281} of AT_1 receptor is essential for full agonism. J Biol Chem;270:12846–12850.
37. Noda K., Saad Y., Karnik S.S. (1995) Interaction of Phe^8 of angiotensin II with Lys^{199} and His^{256} of AT_1 receptor in agonist activation. J Biol Chem;270:28511–28514.
38. Noda K., Saad Y., Kinoshita A., Boyle T.P., Graham R.M., Husain A., Karnik S.S. (1995) Tetrazole and carboxylate groups of angio-

tensin receptor antagonists bind to the same subsite by different mechanisms. J Biol Chem;270:2284–2289.
39. Boucard A.A., Wilkes B.C., Laporte S.A., Escher E., Guillemette G., Leduc R. (2000) Photolabeling identifies position 172 of the human AT_1 receptor as a ligand contact point: receptor-bound angiotensin II adopts an extended structure. Biochemistry;39:9662–9670.
40. Deraet M., Rihakova L., Boucard A., Perodin J., Sauve S., Mathieu A.P., Guillemette G., Leduc R., Lavigne P., Escher E. (2002) Angiotensin II is bound to both receptors AT1 and AT2,'parallel to the transmembrane domains and in an extended form. Can J Physiol Pharmacol;80:418–425.
41. Clement M., Martin S.S., Beaulieu M.E., Chamberland C., Lavigne P., Leduc R., Guillemette G., Escher E. (2005) Determining the environment of the ligand binding pocket of the human angiotensin'II type I (hAT1) receptor using the methionine proximity assay. J Biol Chem;280:27121–27129.
42. Perodin J., Deraet M., Auger-Messier M., Boucard A.A., Rihakova L., Beaulieu M.E., Lavigne P., Parent J.L., Guillemette G., Leduc R., Escher E. (2002) Residues 293 and 294 are ligand contact points of the human angiotensin type 1 receptor. Biochemistry;41:14348–14356.
43. Nikiforovich G.V., Kao J.L.-F., Plucinska K., Zhang W.J., Marshall G.R. (1994) Conformational analysis of two cyclic analogs of angiotensin: implications for the biologically active conformation. Biochemistry;33:3591–3598.
44. The model developed by Dr Laerte Oliveira. Available at: http://www.gpcr.org/7tm/models/oliveira/index.html.
45. Baleanu-Gogonea C., Karnik S. (2006) Model of the whole rat AT_1 receptor and the ligand-binding site. J Mol Model;12:325–337.
46. Ward W.H., Timms D., Fersht A.R. (1990) Protein engineering and the study of structure–function relationships in receptors. Trends Pharmacol Sci;11:280–284.
47. Miura S., Karnik S.S. (2002) Constitutive activation of angiotensin II type 1 receptor alters the orientation of transmembrane helix-2. J Biol Chem;277:24299–24305.
48. Miura S., Zhang J., Boros J., Karnik S.S. (2003) TM2-TM7 interaction in coupling movement of transmembrane helices to activation of the angiotensin II type-1 receptor. J Biol Chem;278:3720–3725.
49. Boucard A.A., Roy M., Beaulieu M.E., Lavigne P., Escher E., Guillemette G., Leduc R. (2003) Constitutive activation of the angiotensin II type 1 receptor alters the spatial proximity of transmembrane 7 to the ligand-binding pocket. J Biol Chem;278:36628–36636.
50. Martin S.S., Boucard A.A., Clement M., Escher E., Leduc R., Guillemette G. (2004) Analysis of the third transmembrane domain of the human type 1 angiotensin II receptor by cysteine scanning mutagenesis. J Biol Chem;279:51415–51423.
51. Urizar E., Claeysen S., Deupi X., Govaerts C., Costagliola S., Vassart G., Pardo L. (2005) An activation switch in the rhodopsin family of G protein-coupled receptors: the thyrotropin receptor. J Biol Chem;280:17135–17141.